

The role of the nonlinearity of the Stefan-Boltzmann law on the structure of radiatively forced temperature change.

MATTHEW HENRY* AND TIMOTHY M. MERLIS

McGill University, Montréal, QC.

ABSTRACT

The Stefan-Boltzmann law, σT^4 , governs the temperature dependence of the blackbody emission of radiation. A consequence of this nonlinearity is that a cold object needs a greater increase in temperature than a hot object in order to reach the same increase in radiation emitted. Therefore, this nonlinearity potentially has an impact on the structure of radiatively forced atmospheric temperature change in both the horizontal and vertical directions. For example, it has previously been argued to be a cause of polar amplification of surface air warming. Here, the role of this nonlinearity is investigated by (i) assessing its magnitude compared to spatial variations in CO₂'s radiative forcing for Earth's atmosphere and (ii) linearizing σT^4 in a gray-radiation atmospheric General Circulation Model (GCM) with an interactive hydrological cycle. Estimates for Earth's atmosphere show that the combination of the Planck feedback and forcing from CO₂, taken in isolation, would produce a tropically amplified warming. Contrary to expectations, climate change simulations with linearized radiation do not have reduced polar amplification of surface air warming relative to the standard GCM configuration. However, simulations with linearized radiation consistently show less warming in the upper troposphere and more warming in the lower troposphere across latitudes. The lapse rate feedback from a pure radiative and radiative-convective configuration of the model are used to show the cold-altitudes-warm-more effect of σT^4 carries across this model hierarchy.

1. Introduction

The change in atmospheric temperature due to radiative forcing is vertically and horizontally inhomogeneous. The zonal-mean pattern of warming is amplified near the surface at the poles and in the upper troposphere in the tropics. Polar amplification (PA) of surface air warming is a common feature of climate model projections (Manabe and Wetherald 1975; Pithan and Mauritsen 2014). Observations of the recent climate also show a faster transient warming rate in the Arctic (Stocker et al. 2013), while Antarctic amplification is transiently delayed as a result of ocean heat uptake (Manabe et al. 1991). In the tropics, there is amplified warming in the upper troposphere relative to the surface in future climate projections that is comparable to that of a warmed moist adiabat (Santer et al. 2005).

There are several mechanisms that are thought to contribute to the pattern of temperature change, and the challenge is to understand the relative importance of each mechanism and the interactions between each of them.

The main contributors to the PA of surface air warming are thought to be the surface albedo feedback (Winton 2006; Graversen et al. 2014), an increase in poleward energy transport (Alexeev and Jackson 2013; Lee 2014; Merlis and Henry 2017), and a destabilizing polar lapse rate feedback (Graversen et al. 2014; Pithan and Mauritsen 2014; Payne et al. 2015). The role of cloud and water vapor feedbacks on the PA of surface air warming is uncertain. According to Pithan and Mauritsen (2014), clouds have a small positive impact on PA and water vapor counteracts PA via their radiative feedbacks. Winton (2006) found that the total longwave feedback (which includes cloud, water vapor, and temperature) contributes to PA. Finally, the top-of-atmosphere (TOA) net radiation response to a vertically invariant temperature change, the Planck feedback, can have spatial structure that tends to amplify polar warming. The structure arises from the nonlinearity of the temperature dependence of the blackbody emission of radiation given by the Stefan-Boltzmann law, σT^4 . For example, while comparing contributions to polar amplification on an aquaplanet from various feedbacks, Langen et al. (2012) found that the Planck and lapse rate feedbacks set up the temperature change pattern that is then amplified with unchanged pattern by the water vapor feedback. Feldl and Roe (2013b) used an aquaplanet slab model with a simple parametrization of the ice albedo

*Corresponding author address: Dept. of Atmospheric and Oceanic Sciences, McGill University, 805 Sherbrooke Street West, Montréal, QC H3A 2K6, Canada.
E-mail: matthew.henry@mail.mcgill.ca

feedback and diagnosed that the latitudinal variation in the Planck feedback contributes to about 20% increase in warming poleward of 60 degrees and about 20% cooling in the subtropics compared to having a homogenized Planck feedback. Pithan and Mauritsen (2014) diagnosed that the Planck feedback contributes 1.7 degrees of warming in the Coupled Model Intercomparison Project Phase 5 (CMIP5) models for an average Arctic warming of 11.1 degrees and cools the tropics by 0.5 degrees for an average warming of 4.5 degrees by analyzing perturbation TOA energy budgets. However, diagnosing the role of a mechanism on regional temperature change using perturbation energy budgets—used in many of these analyses—may lead to a different conclusion than an analysis based on turning off that mechanism in climate models¹ (Merlis 2014).

Radiation also plays a key role in determining the vertical structure of temperature in the troposphere. In high latitudes, radiative cooling is thought to be critical in determining the mean stratification, particularly inversions (Curry 1983). In low latitudes, the troposphere's stratification is close to moist adiabatic, but biases in the climatology of comprehensive General Circulation Models (GCM) and concomitant differences in projected changes may be related to discrepancies in the treatment of radiative processes between GCMs (Po-Chedley and Fu 2012; O'Gorman and Singh 2013). Hence radiation is key in determining the vertical structure of the troposphere at high latitudes and has a possible role in determining the tropical stratification. The nonlinearity of the Stefan-Boltzmann law may then impact the vertical structure of temperature change by making the cold upper layers of the troposphere more sensitive than the warm lower layers.

In this paper, the role of the Stefan-Boltzmann law's nonlinearity on the structure of radiatively forced temperature change is assessed. The Stefan-Boltzmann law has been examined as a stabilizing nonlinearity for the global climate sensitivity under large perturbations (Bloch-Johnson et al. 2015), while our focus is on the role of this nonlinearity on the pattern of global warming, rather than its amplitude. First, the spatial variations of the Planck feedback and CO₂'s radiative forcing for Earth's atmosphere are compared using reanalysis data and a radiative kernel derived from a comprehensive GCM (section 2). We then compare the pattern of warming of an idealized aquaplanet atmospheric GCM (Frieron et al. 2006) with a gray radiation scheme to one that has a linearized version of the gray radiation scheme. It is linearized by replacing σT^4 with $A + BT$ for the radiation scheme's longwave emission source function (section

3). This lets us (i) test the importance of the nonlinearity for polar amplification (section 4) and (ii) assess its effect on the vertical structure of tropospheric warming (section 5). Finally, we use a radiative-convective and a pure radiative configuration of the idealized model to confirm the Stefan-Boltzmann nonlinearity affects the vertical structure of tropospheric warming across a hierarchy of model configurations in which radiation plays an increasingly important role in determining the pattern of temperature change.

2. Patterned warming from Stefan-Boltzmann Law

Taken in isolation, the nonlinearity of the temperature dependence of radiation, σT^4 , is a mechanism for increased warming at cold temperatures. If changes in the oceanic and atmospheric energy transports and all other radiative feedbacks are ignored, the temperature response to a radiative forcing at the top of atmosphere \mathcal{F} is $\Delta T_s = \mathcal{F}/(4\sigma T_s^3)$, where T_s is the surface air temperature². For example, at 303 K, an external forcing \mathcal{F} of 4 W m⁻² can be balanced by a temperature increase of 0.64 K; whereas at 253 K, a 1.1 K warming is required to attain a radiative balance. Hence, if \mathcal{F} is constant over all latitudes, the temperature response is greater at climatologically colder, high latitudes than at climatologically warmer, low latitudes. This is the mechanism by which the spatial structure of the Planck feedback, through the Stefan-Boltzmann law, has been argued to give rise to PA.

The simple argument for the role of the Planck feedback on polar amplification relies on the assumption that the radiative forcing is latitudinally uniform. However, it is important to note that the TOA longwave radiative forcing \mathcal{F} has structure arising from the mean temperature distribution (Zhang and Huang 2014; Payne et al. 2015): the forcing is larger in the tropics than in high latitudes and this counteracts the Planck feedback's tendency for PA. In Payne et al. (2015), a simple one-layer atmospheric model is used to show that the forcing varies with latitude or mean temperature in a way that exactly compensates for the variation in the Planck feedback. In their model, the forcing of a small change in atmospheric emissivity results in the same $(4\sigma T^3)^{-1}$ dependence as the Planck feedback. This implies that if the Planck feedback is the only active feedback and all energy transports are unchanged, the change in temperature induced by the forcing would be uniform in latitude. Feldl and Roe (2013a) also show this in the partial temperature change induced by forcing and normalized by the Planck feedback (their figure 6a). Radiative forcing estimates for carbon dioxide and other well-mixed greenhouse gases have long-been

¹This can account for the differing conclusions between Langen et al. (2012) and Pithan and Mauritsen (2014).

²The difference between the surface air temperature and the skin temperature of the planet depends on turbulent fluxes (e.g., Byrne and O'Gorman 2013).

known to have spatial structure (e.g., Hansen et al. 2005), though consideration of the consequences of this structure on the atmospheric energy transport and circulation changes have only recently been examined (Huang and Zhang 2014; Merlis 2015). Here, we present an analysis of how the spatial structure of radiative forcing affects the meridional structure of the surface air temperature change.

Huang et al. (2016) showed radiative forcing estimates from homogeneous changes in greenhouse gas concentration using the ERA-Interim reanalysis and relate the TOA radiative forcing variations to climatological factors beyond the mean temperature that Payne et al. (2015) discussed. They show that the strength of the forcing is strongly dependent on surface and atmosphere variables, especially the lapse rate. Figure 1 shows the fractional latitudinal variation of instantaneous CO₂ radiative forcing from Huang et al. (2016) (their figure 1c) and the fractional variation of the Planck feedback from the temperature radiative kernel derived from the Geophysical Fluid Dynamics Laboratory AM2 comprehensive atmospheric GCM (Soden et al. 2008, their figure 6). These variations in latitude are also given for the idealized GCM (dashed). If the Planck feedback is the only active feedback and all energy transports are unchanged, the surface air temperature change can be calculated as $\Delta T_s(\phi) = -\mathcal{F}(\phi)/\lambda_P(\phi)$. The simple one-layer atmosphere model described by Payne et al. (2015) would give a uniform ΔT_s . However, as is shown in figure 1, the combination of the Planck feedback and the forcing actually gives a tropically-amplified surface air warming that arises from the greater equator-to-pole variation of the forcing compared to the Planck feedback³. The stronger equator-to-pole variation of the forcing arises primarily from the dependence of the forcing on the climatological lapse rate: the high latitudes have weak forcing because they are closer to the isothermal regime, where there is no greenhouse effect, than low latitudes. The idealized GCM (described in what follows) has a pattern of forcing and Planck feedback variation that is quite similar to the estimates for Earth. In summary, the climatological meridional temperature gradient gives rise to a spatially varying Planck feedback that would, in isolation, cause polar amplified warming. However, this is more than offset by the climatological temperature distribution's effect on the radiative forcing, where both the mean temperature and lapse rate's equator-to-pole decrease produce a tropically amplified forcing.

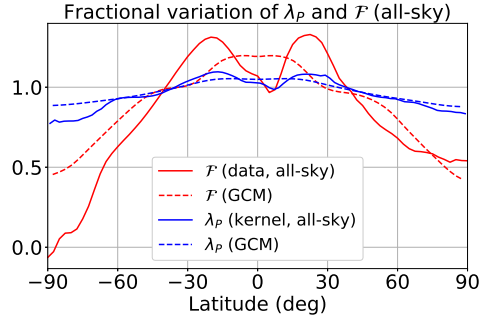


FIG. 1. Fractional variation from the global mean of forcing (\mathcal{F}) and Planck feedback (λ_P) from Earth estimates and the idealized GCM. The idealized GCM is shown in dashed lines. The CO₂ forcing data (solid red) is from Huang et al. (2016) and the Planck feedback (solid blue) was calculated from the annual mean of the temperature radiative kernel derived from GFDL's comprehensive AM2 GCM (Soden et al. 2008).

A similar argument to the one made for the role of the Planck feedback on polar amplification can be made for the vertical dependence of temperature change in response to radiative forcing. The effect of the nonlinearity of σT^4 is that the temperature response of the higher altitude, colder layers of the troposphere is larger, whereas the temperature response of lower altitude, warmer layers is smaller provided the level-by-level emission is the same. Hence, with linearization, the lower altitude layers will be more sensitive and the higher altitude layers will be less sensitive to a given forcing. Therefore, one expects eliminating Stefan-Boltzmann law's nonlinearity to result in a destabilization of the tropospheric stratification relative to nonlinear radiation GCM simulations of radiatively forced warming, in the absence of other changes in the atmospheric heat budget.

We aim to test the effect of the nonlinearity of σT^4 on the vertical and horizontal pattern of warming by linearizing this function in an idealized aquaplanet GCM with a gray radiation scheme. The GCM simulations have additional degrees of freedom beyond the purely radiative mechanism by which the σT^4 nonlinearity gives rise to patterned warming. In particular, advection and convection can give rise to deviations from the expectations described in this section.

3. Idealized GCM

We use the moist idealized GCM described in Frierson et al. (2006) with the modifications and parameter values described in O'Gorman and Schneider (2008). The surface boundary condition is an aquaplanet with a slab mixed layer ocean with the heat capacity of 1 m of water and no representation of ocean heat transport. The GCM's

³In Pitman and Mauritsen (2014), the combination of the Planck feedback and the radiative forcing seems to give a polar amplified warming; however, their diagnosis of the Planck feedback includes the effect of the spatial structure of the surface air temperature change [$\lambda_P(\phi)\Delta T_s(\phi)$]. The spatial structure of T_s , which can arise from a variety of factors, then gives rise to a latitudinal variation in the Planck feedback that is larger than that of the radiative forcing.

spectral dynamical core has T42 spectral truncation for a nominal horizontal resolution of $2.8^\circ \times 2.8^\circ$ and 30 vertical levels. The skin temperature is interactively computed using the surface radiative and turbulent fluxes, which are determined by bulk aerodynamic formulae. A k-profile scheme with a dynamically determined boundary layer height is used to parametrize the boundary layer turbulence. The GCM uses a simplified Betts-Miller convection scheme (Frierson 2007). The large scale condensation is parametrized such that the relative humidity does not exceed one and the condensed water is assumed to immediately return to the surface. Incoming solar radiation is an idealized second Legendre polynomial function that is representative of Earth's annual mean with no seasonal or diurnal cycle. For longwave radiation, the model has gray radiative transfer, with the longwave optical depth as in O'Gorman and Schneider (2008). The radiative fluxes are a function of temperature and pressure alone, so there are no water vapor or cloud feedbacks. The surface has no representation of sea ice and has a uniform surface albedo, so there is no surface albedo feedback. All simulations are 2000 days with time averages over the last 1000 days shown, when all climate states have reached a statistical steady state.

Figure 2a shows the time- and zonal-mean temperature field for the control simulation of the standard configuration of the idealized moist GCM. The temperature field is comparable to that of Earth's annual mean, although the tropospheric lapse rate is everywhere positive and the stratosphere is biased from gray radiation and the absence of ozone. We can, therefore, assess the role of the Stefan-Boltzmann nonlinearity on the pattern of radiatively forced temperature change for a regime similar to that of Earth's climate.

To examine the effect of the Planck feedback on the pattern of warming, the radiation source function, σT^4 , of longwave radiation is replaced with a linear approximation: $A + BT$. Different values for A and B are chosen to test the sensitivity of our result to these constants. The chosen values of A and B are displayed in figure 3's legend. The values of A and B are chosen such that $A + BT$ is tangent to σT^4 at 240K, 250K, 265K and 300K to span the control simulation's temperature field (figure 2a), and these values are then rounded for ease of replication. We also test the sensitivity to changes in A with the same value of B with two more linearizations. When B equal to $4.6 \text{ W m}^{-2} \text{ K}^{-1}$, the simulated temperature change pattern resembles the nonlinear radiation simulation most closely, so we test the sensitivity of the results to variations in A for this value of B . In total, we present six linearizations. We note that none of the simulations reach a low enough temperature to have a negative value for longwave emission ($A + BT > 0$ for all

T). While alternative linear radiation simulations with σT^4 linearized about the spatially varying climatological temperature are possible, it is important that B is constant as the Planck feedback is then spatially uniform and thus has no effect on the horizontal structure of temperature change.

Figures 2a and b show the control temperature field for the nonlinear radiation simulation and a linear radiation simulation ($A = -700 \text{ W m}^{-2}$, $B = 3.7 \text{ W m}^{-2} \text{ K}^{-1}$) respectively. These control temperature fields are broadly similar, although small changes occur due to biases in the longwave radiation emission function as a result of its linearization. The control temperature fields of the linear radiation simulations are comparable, so one of them is chosen here as an example. Figure 3a also shows that the control surface air temperature is sensitive to the A parameter (spread between the three simulations with $B = 4.6 \text{ W m}^{-2} \text{ K}^{-1}$). The A parameter sets the amount of temperature-independent emission of radiation, so a higher A means greater longwave emission and a colder control climate. Figure 3a shows that the control surface air temperature is not so sensitive to variations in B . The B parameter sets the amount of temperature change required for a certain change in emission and has a significant impact on the amount of global warming but not on the control surface temperature.

The radiative forcing due to an increase in greenhouse gas concentration is modelled by increasing the longwave optical depth. In this model, the optical depth at the surface varies in latitude as: $\tau_{eq} + (\tau_{pole} - \tau_{eq}) \sin^2(\phi)$ where τ_{eq} and τ_{pole} are the optical depth at the equator and pole respectively and ϕ the latitude. The control values for τ_{eq} and τ_{pole} are 7.2 and 1.8 respectively. The vertical structure of the optical depth has a component that decays quartically in pressure as σ^4 , mimicking water vapor's scale height, and a component that decreases linearly in pressure as σ , mimicking well-mixed greenhouse gases, where σ is the pressure normalized by the surface pressure (equation 1 of O'Gorman and Schneider 2008). The effect of an increase in greenhouse gas concentrations is represented by a multiplicative increase of the optical depth by a factor of 1.4 for both τ_{eq} and τ_{pole} , which results in a global-average adjusted radiative forcing of 24 W m^{-2} for the nonlinear radiation simulation and from 20 W m^{-2} to 27 W m^{-2} for the linear radiation simulations with some dependence on the linearization coefficients (section 5). The main results of this paper are insensitive to the magnitude of the forcing. A multiplicative increase of 1.1 of the optical depth gives a global mean forcing of 5.9 W m^{-2} , which is similar to a quadrupling of CO_2 . While the magnitude of the forcing is large in the perturbation simulations presented in this paper, the pattern of the forcing is similar to estimates for

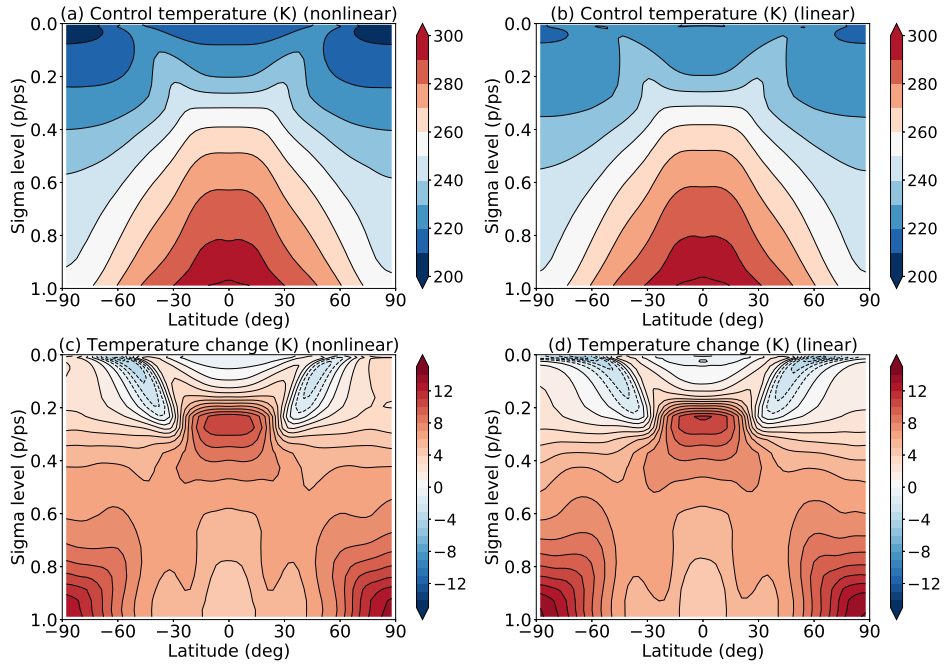


FIG. 2. Control temperature field for the (a) nonlinear radiation simulation and (b) one of the linear radiation simulations ($B = 3.7\text{W m}^{-2}\text{K}^{-1}$, $A = -700\text{W m}^{-2}$). (c) Temperature change field for the simulations with nonlinear radiation and (d) simulations with linear radiation ($B = 3.7\text{W m}^{-2}\text{K}^{-1}$, $A = -700\text{W m}^{-2}$).

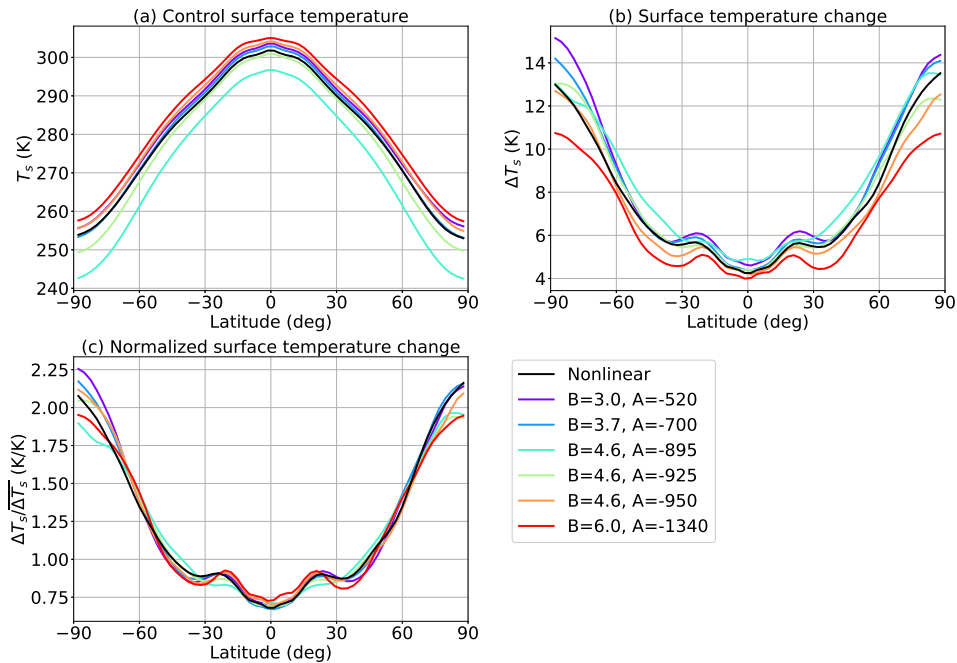


FIG. 3. (a) Surface air temperature for the control simulation with different linearizations. (b) Surface air temperature change between the increased and control optical depth simulations. (c) Surface air temperature change normalized by global-mean surface air temperature change.

Earth (figure 1). There are thus 4 configurations: linear longwave optical depth.
or nonlinear radiation scheme and control or increased

Figures 2c and d show the temperature change field for the nonlinear radiation simulations and corresponding linear radiation simulations. Both temperature change patterns are broadly similar. Despite the idealized nature of the GCM, they are in good agreement with the ensemble-mean pattern of temperature change in the comprehensive GCMs shown in the fifth Assessment Report of the Intergovernmental Panel on Climate Change (IPCC) (Stocker et al. 2013, their figure 12.12); however, figures 2c and d represent temperature change between two equilibrium states while the IPCC figures represent the transient climate response, so the surface air temperature change in the Southern Hemisphere is not polar amplified. The idealized GCM has cooling in part of the stratosphere, though its structure and magnitude may be unrealistic due to the simplicity of this model's radiative transfer scheme.

Figure 3b shows the surface air temperature change between the control and increased longwave optical depth simulations for nonlinear radiation (black) and the different linearizations of σT^4 (colors). The simulated polar warming varies from 11K to 15K in these simulations. However, much of this results from variation in the amount of global warming rather than from variation in the *pattern* of warming. Figure 3c shows the surface air temperature change normalized by its global mean. For all linearizations, the simulated pattern of warming is quite similar to the nonlinear radiation simulation. These experiments then show that the linearization of the radiation scheme does not substantially affect the pattern of surface air warming. The amount of normalized surface temperature change at the poles varies by approximately 15% across the radiation parameters (0.3K/K relative to a total normalized polar warming of 2K/K). This is comparable to the magnitude of the diagnosed role of the Planck feedback for Arctic amplification in the CMIP5 simulations (1.7K relative to a total warming of 11.1K, Pithan and Mauritsen (2014)), but the range of linear radiation simulations includes both those with slightly more and less polar amplified warming. This result therefore contradicts the expectation based on the TOA energy balance: the nonlinearity of σT^4 does not systematically increase the amount of polar amplification of surface air warming.

4. Horizontal structure of warming

We perform a radiative feedback analysis to diagnose both the factors affecting the climate sensitivity and the spatial structures of the different feedbacks. The GCM used in this experiment has gray radiation and a prescribed optical depth, so only the temperature feedback is active, and there are no water vapor, cloud, or surface

albedo feedbacks. The temperature feedback consists of the Planck feedback λ_P and the lapse rate feedback λ_{LR} . The total feedback $\lambda_T = \lambda_P + \lambda_{LR}$ is computed as follows:

$$\lambda_T(\phi) = \frac{-\mathcal{F}(\phi) + \Delta[\nabla \cdot \mathbf{F}_{MSE}(\phi)]}{\Delta T_s(\phi)}, \quad (1)$$

where \mathcal{F} is the radiative forcing, $\Delta[\nabla \cdot \mathbf{F}_{MSE}]$ is the change in the divergence of moist static energy (MSE) flux between the control and increased optical depth simulations which represents the vertically integrated horizontal atmospheric energy transport, ΔT_s is the change in surface air temperature, and ϕ is the latitude. The change in the net TOA radiation is used to calculate the change in divergence of the MSE flux. This is a local feedback analysis where the sum of the forcing and the change in MSE divergence is balanced by the product of the local change in surface temperature and the locally defined climate feedback parameter. This type of local feedback analysis is similar to Boer and Yu (2003), although they divide by the global-mean surface air temperature change, whereas we divide by the local surface air temperature change. These two types of feedback analysis were denoted by Feldl and Roe (2013a) as “global” and “local” definition of the climate feedback, respectively.

To compute the Planck feedback, a second temperature field is initialized at each time step in the GCM's radiation scheme with a temperature value incremented by one Kelvin at the surface and for all of the GCM's vertical levels. The Planck feedback is then computed as the time mean of the difference between the outgoing longwave radiation (OLR) corresponding to the GCM's prognostic temperature field in the control simulation and the OLR corresponding to the temperature field incremented by one. The lapse rate feedback is computed as the residual: $\lambda_{LR} = \lambda_T - \lambda_P$. Therefore, second-order effects that occur because of nonlinearities or large amplitude responses are not separated out (Feldl and Roe 2013b). The feedbacks are very similar in simulations with smaller amplitude forcing, suggesting that the residual calculation of λ_{LR} is accurate.

To calculate the value of the radiative forcing, a new simulation is done where the sea surface temperature (SST) is prescribed to the time- and zonal-mean of the control simulation SST and the optical depth is increased. The change in radiative flux at the top of the atmosphere after the stratospheric and tropospheric temperature has changed directly in response to the optical depth (as opposed to changes mediated by surface temperature variations) defines the troposphere-adjusted radiative forcing (Hansen et al. 2005). This adjusted forcing is a more accurate measure of the radiative forcing and alters our estimate of the lapse rate feedback compared to the instantaneous forcing. This gray radiation model has less

stratospheric cooling than comprehensive climate models. However, the focus of this study is the troposphere and any effect this different stratospheric cooling may have on the troposphere is taken into account by using this adjusted forcing. The latitudinal structure of the troposphere-adjusted radiative forcing of the idealized GCM closely resembles that of instantaneous CO₂ radiative forcing from Huang et al. (2016) (figure 1). We also note that the instantaneous forcing structure from the idealized GCM is similar to the troposphere adjusted forcing structure (not shown).

We diagnostically employ the forcing and feedback analysis of the GCM results by expressing each component's change in the local TOA radiation budget in terms of a surface temperature change. The Planck feedback can be decomposed into its global-mean $\bar{\lambda}_P$ and its deviation from this mean $\lambda_P - \bar{\lambda}_P$. Similar to the analysis of Feldl and Roe (2013b), we diagnose the change in surface air warming by isolating $\bar{\lambda}_P \Delta T_s$ in equation 1 and dividing by $\bar{\lambda}_P$ as follows:

$$\Delta T_s(\phi) = \frac{-\mathcal{F}(\phi) + \Delta[\nabla \cdot \mathbf{F}_{MSE}(\phi)] - \Delta T_s(\phi) \{ \lambda_{LR}(\phi) + [\lambda_P(\phi) - \bar{\lambda}_P(\phi)] \}}{\bar{\lambda}_P(\phi)}, \quad (2)$$

The overline $\bar{(\cdot)}$ indicates an area-weighted global mean. From the left to the right, the four terms in the numerator will be denoted as forcing, transport, lapse rate feedback, and variable Planck feedback, respectively. This type of budget analysis also formed the basis of the quantification of Arctic warming in Pithan and Mauritsen (2014).

Figure 4a shows the area-weighted polar mean ($|\phi| > 60^\circ$) versus the area-weighted tropical mean ($|\phi| < 30^\circ$) of each term of this sum. Tests with different averaging conventions show that results in figure 4 are insensitive to the latitude ranges. The distance to the 1:1 line indicates the forcing or feedback's contribution to polar amplification (Pithan and Mauritsen 2014). The black symbols correspond to the nonlinear radiation simulation and other colors correspond to different linear radiation simulations. We note that if the forcing is increased in a model that has an amplitude-independent warming pattern, the points corresponding to the simulation with increased forcing will be further from the 1:1 line even though the pattern of warming is the same. Likewise, two models with identical warming *patterns*, but different global-mean climate sensitivity would appear to have different degrees of polar amplification on this diagram. Therefore, we normalize all points by the global-mean surface air temperature change in figure 4b and discuss this in what follows.

All linear radiation simulations have a zero variable Planck feedback contribution by definition ($\lambda_P - \bar{\lambda}_P = 0$). The nonlinear radiation simulations' Planck contribution

is above the 1:1 line and contributes to polar amplification according to this energy budget analysis (black x). The lapse rate-related temperature change is stronger in linear radiation simulations than in nonlinear radiation simulations over all latitudes (colored triangles are further up and to the right compared to the black triangle, except for the extreme $B = 3.0 \text{ W m}^{-2} \text{ K}^{-1}$ case) due to the cooler upper tropospheric layers having a higher temperature increase in the nonlinear radiation case. Once normalized, the change in moist static energy transport is similar between linear radiation and nonlinear radiation simulations (except for the extreme $B = 3.0 \text{ W m}^{-2} \text{ K}^{-1}$ case). This is consistent with diffusive closures—the change in moist static energy transport is proportional to the pattern of temperature change (figure 3), all else being equal. The forcing changes slightly between the different simulations—the effect of increasing the optical depth varies depending on the radiation scheme as a result of slight differences in the control simulation temperature field. However, the dominant variation in forcing in figure 4 arises from the generally higher value of $\bar{\lambda}_P(\phi)$ for the linearizations presented here. Therefore, the forcing term $-\mathcal{F}(\phi)/\bar{\lambda}_P(\phi)$ is generally smaller (closer to the origin) in the linear radiation simulations, as can be seen in figures 4a and b. In summary, the Planck feedback functions as expected: it contributes to polar amplification in the nonlinear radiation simulations and has no effect on polar amplification in the linear radiation simulations. According to our budget analysis, this difference could be offset by the change in MSE flux convergence and/or the lapse rate feedback to arrive at a comparable warming pattern (figure 3c). Figure 4b shows there are only modest differences in the MSE flux convergence change between the linear and nonlinear radiation simulations, which we confirmed using both the TOA net radiation and an explicit calculation of the MSE flux convergence from the GCM output. The only other degree of freedom in this GCM is the lapse rate feedback. The difference in the variable Planck feedback contribution between the nonlinear and linear radiation simulations is offset by changes in the lapse rate feedback: the contribution of the lapse rate feedback in the linear radiation simulations is generally toward more polar amplification than in the nonlinear radiation simulation.

The lapse rate feedback contributes to more warming over all latitudes as evidenced by the fact that colored triangles are generally further up and to the right than the black triangle, but it also contributes to more polar amplification of surface air warming as the distance to the 1:1 line of colored triangles is larger than the distance to the 1:1 line of the black triangle. The structure of the lapse rate feedback is discussed in more detail in the next section.

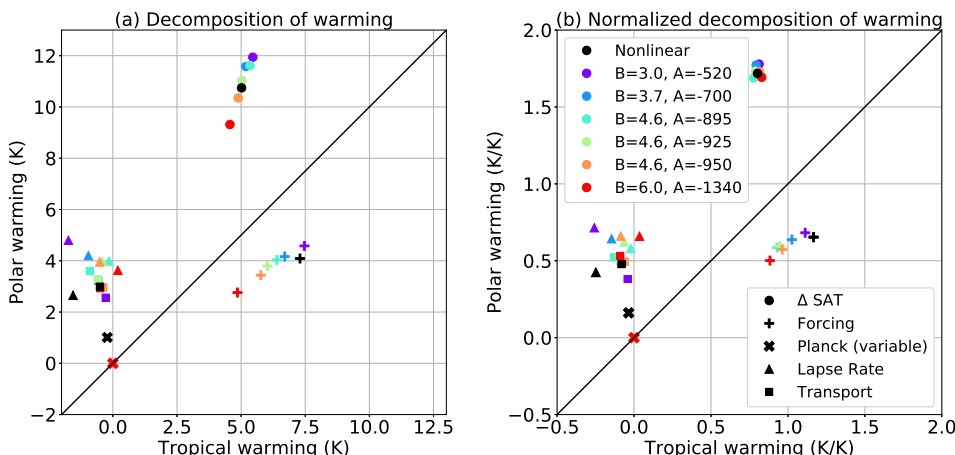


FIG. 4. (a) Energy budget diagnosis of polar ($|\phi| > 60^\circ$) and tropical warming ($|\phi| < 30^\circ$) with changes from spatially varying forcing, the variable Planck feedback, the lapse rate feedback, and the convergence of moist static energy transport (equation (2)). The distance from the 1:1 line (black) indicates the component's contribution to the polar or tropical amplification of warming. (b) Energy budget diagnosis normalized by global-mean surface air temperature change.

5. Global-mean feedbacks and vertical structure of warming

Figure 5 shows the forcing-feedback analysis for the global-mean values of the temperature change ($\overline{\Delta T_s}$), radiative forcing (\mathcal{F}), and radiative feedbacks ($\overline{\lambda_{total}}, \overline{\lambda_P}, \overline{\lambda_{LR}}$) for all simulations. The perturbed simulations have about 6K of global warming that results from a combination of a large global-mean radiative forcing ($\approx 24 \text{ W m}^{-2}$) and a very stabilizing climate feedback parameter ($\approx -4 \text{ W m}^{-2} \text{ K}^{-1}$). A notable feature of figure 5 is that the nonlinear radiation simulation (black) is within the range of values of the linear radiation simulations (color) for all variables except the lapse rate feedback ($\overline{\lambda_{LR}}$). The lapse rate feedback of the nonlinear radiation simulation is smaller than that of the linear radiation simulations (apart from the extreme $B = 3.0 \text{ W m}^{-2} \text{ K}^{-1}$ simulation where the difference is minimal). The importance of the Stefan-Boltzmann nonlinearity on the vertical structure of warming and concomitant effect on $\overline{\lambda_{LR}}$ has not been previously documented, a task that we pursue here.

Figures 6a and b show the area-weighted polar mean ($|\phi| > 60^\circ$) and the area-weighted tropical mean ($|\phi| < 30^\circ$) of the vertical structure of the temperature change normalized by the surface air temperature change for the nonlinear radiation simulation (black) and the linear radiation simulations (colors). The nonlinear radiation simulation shows smaller lapse rate increase near the poles and a larger lapse rate decrease in the tropics (except in the upper troposphere for the extreme $B = 3.0 \text{ W m}^{-2} \text{ K}^{-1}$ case). Figure 6c confirms this by showing that the lapse rate feedback of the linear radiation

simulations are generally more positive than the nonlinear radiation simulation across all latitudes, aside from the simulation with $B = 3.0 \text{ W m}^{-2} \text{ K}^{-1}$. The values for the nonlinear radiation simulation can be compared to the CMIP5 multi-model mean (Feldl and Bordoni 2016, their figure 1). The nonlinear radiation simulation has a value at the equator close to $-2 \text{ W m}^{-2} \text{ K}^{-1}$ and a value at the pole of $1 \text{ W m}^{-2} \text{ K}^{-1}$, a somewhat larger equator-to-pole variation than the multi-model mean, which varies from $-1.5 \text{ W m}^{-2} \text{ K}^{-1}$ to $0.8 \text{ W m}^{-2} \text{ K}^{-1}$ (in the Northern Hemisphere). The transition from negative to positive lapse-rate feedback occurs closer to the equator in all of the idealized GCM simulations, though the midlatitudes, where the transition occurs, are not a focus of this study.

That radiation can meaningfully affect the tropical lapse rate change under warming is perhaps surprising given that it is outside the scope of moist adiabat arguments. The role of radiation on tropical lapse rate change bears additional attention given our results and the comprehensive GCM simulations of Mauritsen et al. (2013), where there is distinctive vertical structure to the tropical temperature change in response to changes in cloud radiative effects compared to simulations with changes from CO_2 in isolation of changes in cloud radiative effects.

In order to better understand the impact of linearizing σT^4 on the lapse rate feedback, a radiative-convective equilibrium configuration and a pure radiative equilibrium configuration of the GCM are analyzed. Figure 7 shows the lapse rate feedback for the three different configurations of the GCM in the nonlinear radiation case and a linear ($B = 3.7 \text{ W m}^{-2} \text{ K}^{-1}$, $A = -700 \text{ W m}^{-2}$) radiation case, chosen as it has a lapse rate feedback close to the

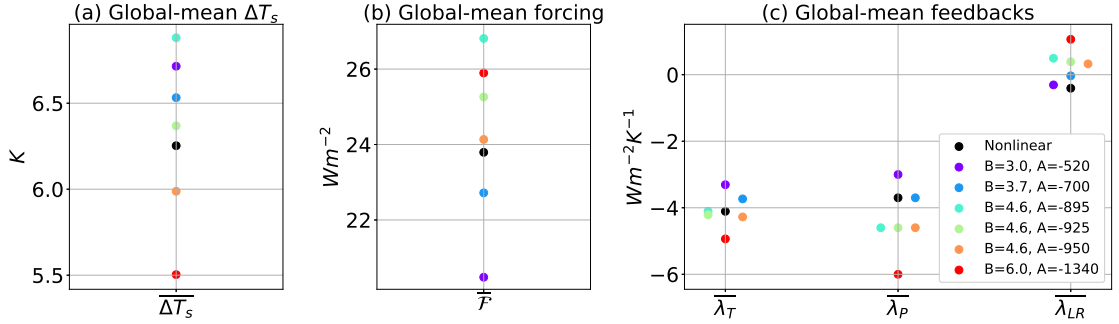


FIG. 5. Global-mean surface air temperature change ($\overline{\Delta T_s}$) (a), global-mean radiative forcing ($\overline{\mathcal{F}}$) (b), and global-mean radiative feedbacks ($\overline{\lambda_T}, \overline{\lambda_P}, \overline{\lambda_{LR}}$) (c) for all simulations.

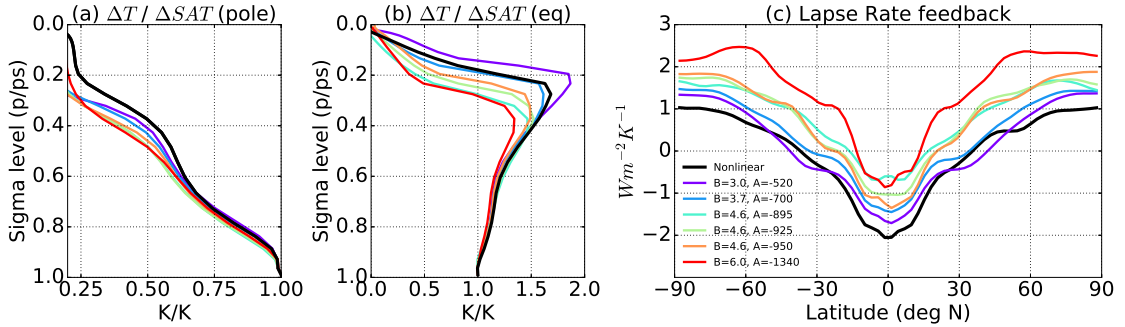


FIG. 6. Area-weighted polar mean ($|\phi| > 60^\circ$) (a) and the area-weighted tropical mean ($|\phi| < 30^\circ$) (b) of the vertical structure of the temperature change normalized by the surface air temperature change for the nonlinear radiation simulation (black) and the linear radiation simulations (color). (c) Lapse rate feedback vs. latitude for all simulations.

nonlinear radiation case. In the radiative equilibrium (Rad Eq) configuration of the GCM, the convection and advection processes are deactivated. The vertical temperature profile is thus determined only by how the longwave radiation of each column balances the absorbed solar radiation. In this configuration, the lapse rate feedback is destabilizing over all latitudes and the nonlinear case has a less destabilizing feedback as the colder upper layers of the atmosphere need a higher increase in temperature to reach the same increase in emission of longwave radiation. The radiative-convective equilibrium (RCE) configuration follows the method described in O’Gorman and Schneider (2008). Since the pure radiative and radiative-convective configurations are effectively column models, we choose to arrange the columns to have the same control surface air temperature as the full GCM configuration. This is nearly equivalent to altering the insolation in the column models to make their surface air temperature match the control GCM simulation, though the optical depth at a given latitude also differs between the column models and the GCM. Convection lessens the difference in lapse rate feedback between the linear and nonlinear radiation cases in the tropics to approximately $0.2 \text{ W m}^{-2} \text{ K}^{-1}$. However, a difference of about $1 \text{ W m}^{-2} \text{ K}^{-1}$ remains in the polar regions. The difference

in lapse rate feedback between the linear and nonlinear radiation simulations in the full GCM configuration is reduced near the poles to approximately $0.3 \text{ W m}^{-2} \text{ K}^{-1}$ and slightly increased in the tropics compared to the radiative convective equilibrium configuration. For the linear and nonlinear radiation cases, the lapse rate feedback is less stabilizing in the full GCM configuration than in the RCE configuration over all latitudes except the tropics.

Presenting the lapse rate feedback across this range of atmospheric model configurations shows that the initial difference in lapse rate feedback between the linear and nonlinear radiation cases in the radiative equilibrium configuration, which is readily understood (section 2), propagates to the full GCM. This difference is, however, attenuated by the other processes involved in the vertical structure of temperature change: convection and advection. Furthermore, this model hierarchy clearly shows the crucial role convection plays in determining the sign of the lapse rate feedback by bringing the warming maximum to the upper troposphere in the tropics. The lapse rate feedback in polar regions, in contrast, is less affected by convection and advection, suggesting that radiation is a key factor in determining the changes in the

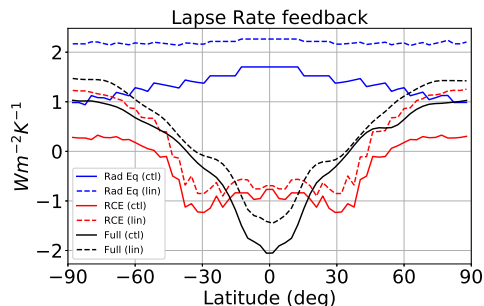


FIG. 7. Lapse rate feedback for three configurations: pure radiative equilibrium (Rad Eq), radiative-convective equilibrium (RCE), and full GCM. For each configuration, the nonlinear radiation simulation case (ctl) and a linear radiation simulation case are shown (lin).

vertical stratification of temperature at high latitudes.

6. Conclusion

Isolating the factors governing the inhomogeneous pattern of atmospheric temperature change is a central problem in climate dynamics, with implications for the atmospheric general circulation and regional climate changes. Here, we assess the role of the nonlinearity of the Stefan-Boltzmann law σT^4 in determining the pattern of radiatively forced warming. It had previously been suggested to augment polar amplification by giving rise to the spatial structure of the Planck feedback. Beyond the spatial pattern of surface warming, we show that the nonlinearity of the Stefan-Boltzmann law affects the vertical structure of atmospheric temperature change in a manner that tends to make the lapse rate feedback more stabilizing.

If all other radiative feedbacks are neglected and energy transports do not change, the nonlinearity of σT^4 implies that the temperature response to a given forcing is higher for a lower mean temperature and lower for a higher mean temperature. Given that the poles are colder than the equator, this is a reason to expect a greater temperature response at higher latitudes, as recent energy budget analyses of GCMs have found. However, the climatological atmospheric temperature also underlies the equator-to-pole radiative forcing contrast, which is sufficient to produce tropically amplified warming if atmospheric and oceanic energy transports do not change and only the spatially varying Planck feedback and forcing are considered (figure 1). Analogous reasoning for the Stefan-Boltzmann nonlinearity can also be applied in the vertical dimension: given that higher altitudes of the troposphere are colder, it is expected that they have a greater temperature response. We linearize the temperature dependence of the blackbody emission of radiation, σT^4 , in an idealized aquaplanet GCM with a

gray radiation scheme to assess the role of the nonlinearity of σT^4 on the structure of temperature change.

The results from the linear radiation simulations do not systematically show less polar amplification of surface air warming. Hence, in these experiments, the nonlinearity of σT^4 does not augment the polar amplification of the surface air warming. Other components of the changing local energy budget such as a change in the moist static energy flux convergence or the lapse rate feedback can offset the tendency for the spatial structure of the Planck feedback toward polar amplified warming. In these GCM simulations, the lapse rate feedback contributes to more polar amplification in the linear radiation simulations, which makes up for the expected decrease in warming at the poles from homogenizing the Planck feedback by linearizing σT^4 . We note that the control temperature in our simulations does not have a high latitude inversion, unlike the Earth's climatology. Having a high latitude inversion would make the climatological vertical structure of temperature more homogeneous and this would reduce the high-latitude lapse rate feedback's sensitivity to linearizing radiation.

The results also show a higher lapse rate feedback across all latitudes in the linear radiation simulations. This suggests that the Stefan-Boltzmann nonlinearity is responsible for increasing the temperature response of the colder upper troposphere and reducing the temperature response of the warmer lower troposphere. We confirm this by looking at the lapse rate feedback of a pure radiative and radiative-convective configuration of the GCM. The difference in the lapse rate feedback between the linear and nonlinear radiation simulations in the pure radiative configuration is well understood: the cold upper layers of the troposphere warm more in the nonlinear radiation simulations. This difference then propagates to the full GCM configuration, although it is attenuated by advection and convection. The sensitivity of the magnitude of the tropical upper tropospheric warming to the treatment of radiative transfer in these idealized GCM simulations is noteworthy and suggests further examination in radiation's role on the tropical stratification.

Acknowledgments. This work was supported by the Fonds de Recherche du Québec — Nature et Technologies (FRQNT) Nouveau Chercheur and Natural Sciences and Research Council (NSERC) Discovery grants, as well as a Compute Canada allocation. We would like to thank Yi Huang for providing the CO₂ radiative forcing, Brian Soden for providing the AM2 radiative kernel, Paul O’Gorman for providing the RCE code, Kyle Armour and

Tim Cronin for helpful discussions. We thank an anonymous reviewer for encouraging the use of adjusted radiative forcing.

References

- Alexeev, V. A., and C. H. Jackson, 2013: Polar amplification: is atmospheric heat transport important? *Clim. Dyn.*, **41**, 533–547.
- Bloch-Johnson, J., R. T. Pierrehumbert, and D. S. Abbot, 2015: Feedback temperature dependence determines the risk of high warming. *Geophys. Res. Lett.*, **42** (12), 4973–4980.
- Boer, G., and B. Yu, 2003: Climate sensitivity and response. *Clim. Dyn.*, **20**, 415–429.
- Byrne, M. P., and P. A. O’Gorman, 2013: Land-ocean warming contrast over a wide range of climates: Convective quasi-equilibrium theory and idealized simulations. *J. Climate*, **26**, 4000–4016.
- Curry, J., 1983: On the formation of continental polar air. *J. Atmos. Sci.*, **40** (9), 2278–2292.
- Feldl, N., and S. Bordoni, 2016: Characterizing the Hadley circulation response through regional climate feedbacks. *J. Climate*, **29** (2), 613–622.
- Feldl, N., and G. H. Roe, 2013a: Four perspectives on climate feedbacks. *Geophys. Res. Lett.*, **40**, 4007–4011.
- Feldl, N., and G. H. Roe, 2013b: The nonlinear and nonlocal nature of climate feedbacks. *J. Climate*, **26**, 8289–8304.
- Frierson, D. M., 2007: The dynamics of idealized convection schemes and their effect on the zonally averaged tropical circulation. *J. Atmos. Sci.*, **64** (6), 1959–1976.
- Frierson, D. M. W., I. M. Held, and P. Zurita-Gotor, 2006: A gray-radiation aquaplanet moist GCM. Part 1: Static stability and eddy scale. *J. Atmos. Sci.*, **63**, 2548–2566.
- Graversen, R. G., P. L. Langen, and T. Mauritsen, 2014: Polar amplification in CCSM4: Contributions from the lapse rate and the surface albedo feedbacks. *J. Climate*, **27**, 4433–4450.
- Hansen, J., and Coauthors, 2005: Efficacy of climate forcings. *J. Geophys. Res.*, **110**, D18 104.
- Huang, Y., X. Tan, and Y. Xia, 2016: Inhomogeneous radiative forcing of homogeneous greenhouse gases. *J. Geophys. Res.: Atmospheres*, **121** (6), 2780–2789.
- Huang, Y., and M. Zhang, 2014: The implication of radiative forcing for poleward energy transport. *Geophys. Res. Lett.*, **41**, 1665–1672.
- Langen, P. L., R. G. Graversen, and T. Mauritsen, 2012: Separation of contributions from radiative feedbacks to polar amplification on an aquaplanet. *J. Climate*, **25**, 3010–3024.
- Lee, S., 2014: A theory for polar amplification from a general circulation perspective. *Asia-Pac. J. Atmos. Sci.*, **50**, 31–43.
- Manabe, S., R. Stouffer, M. Spelman, and K. Bryan, 1991: Transient responses of a coupled ocean–atmosphere model to gradual changes of atmospheric CO₂. Part 1. annual mean response. *J. Climate*, **4** (8), 785–818.
- Manabe, S., and R. T. Wetherald, 1975: The effects of doubling the CO₂ concentration on the climate of a general circulation model. *J. Atmos. Sci.*, **32**, 3–15.
- Mauritsen, T., R. G. Graversen, D. Klocke, P. L. Langen, B. Stevens, and L. Tomassini, 2013: Climate feedback efficiency and synergy. *Clim. Dyn.*, 2539–2554.

- Merlis, T. M., 2014: Interacting components of the top-of-atmosphere energy balance affect changes in regional surface temperature. *Geophys. Res. Lett.*, **41**, 7291–7297.
- Merlis, T. M., 2015: Direct weakening of tropical circulations from masked CO₂ radiative forcing. *Proc. Nat. Acad. Sci.*, **112**, 13 167–13 171.
- Merlis, T. M., and M. Henry, 2017: Simple estimates of polar amplification in moist diffusive energy balance models. *J. Climate*, submitted.
- O’Gorman, P. A., and T. Schneider, 2008: The hydrological cycle over a wide range of climates simulated with an idealized GCM. *J. Climate*, **21** (15), 3815–3832.
- O’Gorman, P. A., and M. S. Singh, 2013: Vertical structure of warming consistent with an upward shift in the middle and upper troposphere. *Geophys. Res. Lett.*, **40** (9), 1838–1842.
- Payne, A. E., M. F. Jansen, and T. W. Cronin, 2015: Conceptual model analysis of the influence of temperature feedbacks on polar amplification. *Geophys. Res. Lett.*, 9561–9570.
- Pithan, F., and T. Mauritsen, 2014: Arctic amplification dominated by temperature feedbacks in contemporary climate models. *Nat. Geosci.*, **7**, 181–184.
- Po-Chedley, S., and Q. Fu, 2012: Discrepancies in tropical upper tropospheric warming between atmospheric circulation models and satellites. *Environ. Res. Lett.*, **7** (4), 044 018.
- Santer, B. D., and Coauthors, 2005: Amplification of surface temperature trends and variability in the tropical atmosphere. *Science*, **309** (5740), 1551–1556.
- Soden, B. J., I. M. Held, R. Colman, K. M. Shell, J. T. Kiehl, and C. A. Shields, 2008: Quantifying climate feedbacks using radiative kernels. *J. Climate*, **21**, 3504–3520.
- Stocker, T. F., and Coauthors, Eds., 2013: *Climate Change 2013: The Physical Science Basis*. Cambridge University Press, Cambridge and New York.
- Winton, M., 2006: Amplified Arctic climate change: What does surface albedo feedback have to do with it? *Geophys. Res. Lett.*, **33**, L03 701.
- Zhang, M., and Y. Huang, 2014: Radiative forcing of quadrupling CO₂. *J. Climate*, **27**, 2496–2508.